Fission-product formation in the thermal-neutron-induced fission of odd Cm isotopes

I. Tsekhanovich, N. Varapai,* V. Rubchenya,† D. Rochman,‡ and G. S. Simpson
Institut Laue-Langevin, 38042 Grenoble, France

V. Sokolov
Petersburg Nuclear Physics Institute, 188350 Gatchina, Russia

G. Fioni
Commissariat à l'Energie Atomique, Siège, 75752 Paris Cédex 15, France

Ilham Al Mahamid
Lawrence Berkeley National Laboratory, Berkeley, California 94720, USA
(Received 24 June 2004; published 19 October 2004)

Thermal-neutron-induced fission of ^{243}Cm was studied at the Lohengrin mass separator. The light-mass peak of the fission-yield curve was investigated, and yields of masses from $A=72$ to $A=120$ were obtained. Independent-product yields were determined for nuclear charges $Z=28-37$. The yield of masses in the superasymmetric region was found to be identical to other fission reactions studied at Lohengrin. The multimodal approach to fission and the macroscopic-microscopic method for the calculation of charge-distribution parameters in isobaric chains were used to analyze experimental results from the fission of ^{243}Cm and ^{245}Cm. A systematics on fission modes was derived from the analysis and extended to the ^{247}Cm case. The weight of the ^{132}Sn mode was found to decrease in ^{243}Cm, relative to the ^{245}Cm nucleus. A prediction of the ^{78}Ni yield in the fission of Cm isotopes was made. The feasibility of the study of ^{78}Ni at Lohengrin has been demonstrated.

DOI: 10.1103/PhysRevC.70.044610 PACS number(s): 25.85.Ec, 24.75.+i, 21.10.Gv, 21.10.Ft

I. INTRODUCTION

Precise measurements of nuclear charge and mass distributions from fission reactions deliver valuable information on the dynamics of the fission process. Nowadays, the high level of interest in fission studies is connected with the investigation of fission-fragment yield in the superasymmetric mass region (below $A=80$). Studies in this mass region aim to answer the questions of how the fission process is governed at mass splits with extreme asymmetry and what are the limits for producing very-neutron-rich nuclei. Among the latter, a reliable estimate is extremely important for the production cross section of ^{78}Ni, the study of which will be one of the highlights of modern nuclear physics. Of special interest is also the search for the superasymmetric fission mode.

The superasymmetric mass region is difficult to access experimentally; for thermal-neutron-induced fission, the yield of very light fission products decreases rapidly and at about $A=70$ becomes comparable with that of heavy particles from ternary fission. Experimental studies on thermal-neutron-induced fission made at the Lohengrin mass separator at the Institut Laue-Langevin in Grenoble [1] during recent years, for a number of fissile nuclei, have extended the experimental knowledge of isotopic and fragment-mass behavior down to approximately $A=70$. This brought to light a discontinuity in the fission-product mass-yield curve around mass $A=70$, which was explained by the importance of the Ni shell in this mass region (see Ref. [2] for a review of the experimental results). For masses below $A=70$, the data from the fission of actinide nuclei are practically nonexistent for reactions induced by low-energy neutrons; it is a real *terra incognita*.

This information is, however, important for the development of radioactive nuclear beam (RNB) facilities. To get access to it, further experimental efforts as well as some theoretical-model predictions are required. To develop the latter, again, a comprehensive set of precise experimental data for the fission-product yields close to the limits is highly desired. Reliable data on fission-product yields are also important for the energy production, transmutation, and incineration scenarios of nuclear wastes in hybrid reactors [3].

In the present study, we have investigated thermal-neutron-induced fission of the ^{243}Cm isotope. The present measurement concentrates on the light-mass peak of the fission-yield curve ($A=72-120$) and mainly includes results on the mass yields. The yields of individual nuclei could be obtained only for the lightest masses (from $A=72$ to $A=90$ and $Z=28-37$). The present experimental data were compared with the data recently obtained for the ^{245}Cm nucleus [2,4]. Data sets for both Cm isotopes were then used to disclose systematic trends for mass yields and isotopic and isobaric distributions in the superasymmetric mass region and to extend them to the ^{247}Cm case. This has been achieved in the framework of a multimodal approach to fission [5] and

*Currently at CEA Cadarache, DEN/DER/SPRC/LEPh, 13108 Saint-Paul-Lez-Durance Cédex, France.
†On leave from Khlopin Radium Institute, 194021 Saint-Petersburg, Russia.
‡Present address: Los Alamos National Laboratory, LANSCE-3, Los Alamos, NM 87545, USA.

by developing a method for the calculation of the charge-distribution parameters in isobaric chains.

In the first section, a short description of the experimental setup is given, with special attention paid to the data analysis. Section II is about the theoretical-model analysis used to describe the experimental results obtained. The main results of the study (yields of masses and of individual nuclei) are presented and discussed in Sec. III, along with the data on the ^{245}Cm isotope. It also includes some predictions made for the ^{247}Cm target nucleus, on the formation probability for neutron-rich Ni isotopes. The last section gives a brief summary of the present study.

II. EXPERIMENTAL SETUP AND DATA ANALYSIS

The experiment was performed at the Lohengrin mass separator of the Institute Laue-Langevin (ILL) in Grenoble [1], where a flux of 5.3×10^{14}cm^{-2} s^{-1} of thermal neutrons is available for fission studies. The ^{243}Cm targets were prepared by the electroplating technique at the Lawrence Berkeley National Laboratory. The target material containing some admixtures of americium isotopes (^{243}Am and ^{241}Am) was deposited on a Ti backing. The ratio ^{243}Cm/^{243}Am/^{241}Am was 1/0.27/0.0566 and 1/0.49/0.0476 for the two targets used. Though the amount of ^{243}Am was significant, the direct contribution of this isotope to the mass and isotopic yields measured in the experiment was practically negligible due to its low fission and neutron-capture cross sections. The (n,f) reaction was also unfavorable in the case of ^{241}Am. The $(2n,f)$ reaction could be neglected for this isotope, too, because of its small amount in the target material. To limit the contribution from fission of compound nucleus ^{245}Am*, bred from the initial ^{243}Am, to a negligibly low level (less than 10%), the irradiation time in the neutron beam for each target was limited to 1 week. The target-material thickness was about 110 μg/cm^2, and the targets were covered with a thin nickel foil (thickness of 0.25 μm) to prevent sputtering of the fissile material by fission fragments. The energy loss of the fragments in the target material (half its thickness) and Ni was calculated, for each mass measured, with the computer program TRIM (transport of ions in matter) [6] to be about 8 MeV (~7 MeV in covering foil and ~1 MeV in target). The loss of energy in the half target thickness was taken as an uncertainty corresponding to its full thickness.

When exposed to the thermal-neutron flux, both the fissile material and the covering foil evolve with irradiation time. This evolution manifests itself in changes of moments of the fragment kinetic-energy distribution. Measured daily for a chosen mass, the evolution of targets (burn-up, thermal diffusion into the backing, and oxidation of the Ni foil) could be reliably monitored. The target burn-up behavior could be described by an exponential function. Its value deduced from the experiment was practically the same for both targets and amounted to approximately 5.6 d, whereas the target half-life in the Lohengrin neutron flux, calculated with fission and neutron-capture cross sections from [7], is 19.7 d. The disagreement is significant and cannot be explained by possible inaccuracies in the cross-section data. Presumably, the much shorter experimental half-life was due to considerable "unnatural" losses of fissile material, such as sputtering. Nevertheless, the description of the change with time of fission rates could be adequately fitted by an exponential function as shown in Fig. 1. The burn-up points in Fig. 1 show a smooth behavior, thus indicating that there were no uncontrolled losses of fissile material, which could have affected the experimental results.

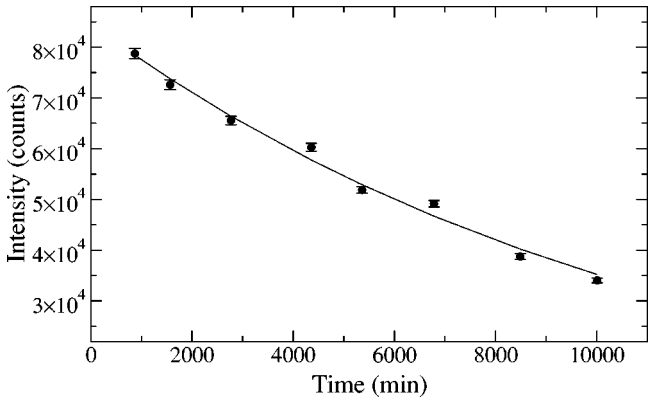

FIG. 1. Experimental burn-up data (points) obtained from the integration of the $A=100$ kinetic-energy distribution. The solid line is a fit with one-exponential function.

The fission fragments were separated in the Lohengrin mass separator according to their mass-to-ionic charge A/q and kinetic energy-to-ionic charge E/q ratios and detected in an ionization chamber. In the $\Delta E-E$ mode, the Frisch-gridded ionization chamber, apart from a distinct resolution of mass multiples (the same A/q and E/q ratios), allowed separation of isobaric-chain members at lightest masses ($A=72-90$). An example of the spectra taken with the ionization chamber is presented in Fig. 2.

The target material (fissile layer and Ni foil) is thin and does not make any significant changes to the initial distribution of ionic charge states of the primary fission fragments

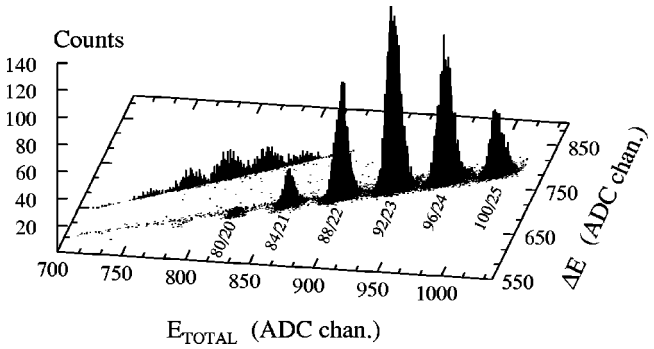

FIG. 2. Fission-product mass scatter plot, taken with an ionization chamber in ΔE-E mode at the separator settings $A/q=4$ and $E/q=4.5$, plotted in coordinates of "specific energy loss ΔE, total kinetic energy E_{TOTAL}." Measuring time was 25 min. The numbers under the peaks (masses) are the mass A/q parameters. Events forming the diagonal line ($E_{\mathrm{TOTAL}}\approx\Delta E$) and the tail under it are, respectively, the fragments stopped in collisions with the separating grid placed between the two ΔE anode sections and those scattered from it.

arising from the division of the electronic shell of a compound nucleus. This determines the electronic (ionic) charge state of fission fragments to be one of the variables which needs to be scanned at the Lohengrin mass separator, to obtain the fragment yield. The second variable is the fragments' kinetic energy which shows a spread of ~15 MeV for the light-fragment group. The spread in kinetic energy for a given mass is a sum product of the fission-process dynamics (deformation at scission point), its isobaric composition, and the fragment slowing-down process in the target material. In the experiment, for each mass, a set of measurements was performed for a number of most probable ionic-charge states (from 18^+ to 24^+) and over an energy span of approximately 30 MeV. For the lightest masses ($A<76$), only one ionic-charge state could be measured, due to low count rates. The same holds for their energy distribution, where only a span of 15 MeV could be covered. For every measurement, count rates were corrected for energy dispersion and burn-up of targets, as well as for the ionic charge-state distributions; a detailed description of the correction can be found in Ref. [8].

An integration over the fission-fragment kinetic-energy distributions has provided a set of relative count rates $I(A)$, which were converted into absolute values $Y(A)$ by normalization of the light-peak yield to 100%. For the masses $A=72-90$, the independent-product yields could be resolved from the fit with multiple Gaussians, after the projection of the corresponding mass spots onto the ΔE axis (Fig. 2). The results for the yields of masses ($A=72-120$) and of the individual isotopes ($A=72-90$) are given and discussed in Sec. IV.

III. THEORETICAL MODEL ANALYSIS

The independent yield of fission fragments Y_{ind} is defined as the yield of a specific fission product after prompt neutron emission from the excited primary fragments emerging from the fission of a compound nucleus with mass A_c, charge Z_c, and excitation energy E_c:

$$Y_{ind}(A,Z,A_c,Z_c,E_c) = \sum_n P_n(A+n,Z,A_c,Z_c,E_c)P_{pre}(Z,A+n,A_c,Z_c,E_c)Y_{pre}(A+n,A_c,Z_c,E_c), \quad (1)$$

where $P_n(A+n,Z,A_c,Z_c,E_c)$ represents the probability of prompt neutron emission from a fragment with mass $A+n$ and charge Z, $P_{pre}(Z,A+n,A_c,Z_c,E_c)$ represents a charge distribution of the $(A+n)$ isobaric chain, and $Y_{pre}(A+n,A_c,Z_c,E_c)$ represents a primary fission-fragment mass distribution.

At low excitation energies, the primary fission-fragment mass and charge distributions exhibit odd-even staggering. The primary distributions can be presented in the factorized form

$$P_{pre}(Z) = \tilde{P}_{pre}(Z)F_{oe}(Z),$$

$$Y_{pre}(A) = \tilde{Y}_{pre}(A)F_{oe}(A), \quad (2)$$

where $\tilde{P}_{pre}(Z)$ and $\tilde{Y}_{pre}(A)$ are smoothed distributions, and the functions $F_{oe}(Z)$ and $F_{oe}(A)$ describe odd-even staggering. The method for modeling the smoothed mass distribution is based on the multimodal nature of nuclear fission [5], depicting the influence of nuclear-shell structure on the potential-energy surface (PES) of fissioning nucleus. The fission process is most probably guided by valleys and bifurcation points of the PES from the equilibrium shape to the scission point. For heavy actinides (from Th to Cf), the so-called standard fission modes (symmetric, spherical ^{132}Sn, and deformed $N=86-90$ shells) have been used. In the case of spontaneous and thermal-neutron-induced fission, these standard modes have to be extended with two additional modes, to better approximate the smoothed primary-mass distribution in the superasymmetric mass region:

$$\tilde{Y}_{pre}(A) = C_{\mathrm{SY}}Y_{\mathrm{SY}}(A) + C_{\mathrm{SI}}Y_{\mathrm{SI}}(A) + C_{\mathrm{SII}}Y_{\mathrm{SII}}(A) + C_{SA1}Y_{SA1}(A) + C_{SA2}Y_{SA2}(A). \quad (3)$$

Here, Y_{SY} and $Y_{\mathrm{SI}}, Y_{\mathrm{SII}}, Y_{SA1}$, and Y_{SA2}, are symmetric and asymmetric components, correspondingly, which present contributions from the different fission modes. Each asymmetric component consists of two peaks representing the heavy- and light-fragment-mass groups and is normalized to unity. The component Y_{SI} is connected with magic numbers $Z=50$ and $N=82$ in heavy fragments, and the superasymmetric components Y_{SA1} and Y_{SA2} are influenced by the $N=50$ and $Z=28$ nuclear shells in the light fragments. The asymmetric mode Y_{SII} is supposed to be connected with a "deformed" nuclear shell at $N=86-90$. The competition between fission modes is determined by fission dynamics and nuclear shells in the fission fragments. The coefficients C_i in Eq. (3) were obtained by comparison with experimental data for the ^{243,245}Cm targets.

In the previous analysis of the fission-product yields at intermediate energies [9], both light and heavy peaks were approximated with Gaussian distributions. However, our analysis of Lohengrin data, which are very precise, has shown that such an approximation is not correct at a large deviation from the peak center. The Gaussian distribution corresponds to the harmonic approximation of the free energy near the bottom of the valley. To take into account the anharmonicity correction, the mass dependence of the variation σ_A was introduced for two asymmetric fission modes (SI and SII) in the form

$$\sigma_A^i(A) = \sigma_A^i(A_i)(1 - c_i^{as(sy)}|A - A_i|), \quad (4)$$

where A_i is an averaged mass of the fission mode and $c_i^{as(sy)}$ is an adjusted parameter which can be different for the two slopes of the Gaussian distribution. This method makes it possibile to suppress the contributions of standard asymmetric modes in the symmetric and superasymmetric mass regions.

Since the smoothed preneutron emission isobaric-charge distribution is approximated by a Gaussian distribution, the odd-even structure can be described by a parameter defined as a third difference of the natural logarithms of the fractional yields [10]. If we consider the proton and neutron odd-even effect separately, one can write

$$F_{oe}(Z) \sim \exp[(\Pi_Z^H + \Pi_Z^L)\,\delta_Z(A_c,Z_c,E_c)], \tag{5}$$

where Π_Z^H and Π_Z^L are defined by the parity of the proton number in the two primary fragments ($\Pi_Z=1$ if Z is even and $\Pi_Z=-1$ if Z is odd). The proton odd-even difference parameter $\delta_Z(A_c,Z_c,E_c)$ is parametrized as a function of excitation energy, charge, and mass number of the compound nucleus in accordance with experimental data [11]. Odd-even staggering in the primary-mass distribution is described by a combination of proton and neutron odd-even effects. The proton and neutron odd-even difference parameters are taken to be proportional—i.e., $\delta_N(A_c,Z_c,E_c)=\text{const} \times \delta_Z(A_c,Z_c,E_c)$, with const$\sim 0.5$.

The average value and variation of the smoothed charge distribution of the primary fragments was calculated in the framework of the scission-point model [12]. The mean charge of the primary isobaric chain $\overline{Z}(A)$ was defined at the minimum of the smoothed potential energy at the scission point for members of the isobaric chain including shell and pairing effects. To calculate the charge variation $\sigma_Z(A)$, the model of a frozen quantal fluctuation of charge asymmetry degree of freedom [13] was used. The stiffness of the harmonic potential for the charge collective coordinate has been obtained by an approximation of the calculated potential energy at the scission point. For the inertia parameter of the charge collective coordinate, the expression derived in Ref. [14] was used.

To calculate the neutron-emission probability from the primary fragments, a simplified statistical description was used. The neutron multiplicity distribution can be approximated by Gaussians [15]. The averaged prompt-neutron multiplicity is proportional to the excitation energy of the fragment, which was calculated using a scission-point model. The calculation of the variation of the excitation energy is a more complex problem. Therefore, an approximated relation between the standard variation and neutron multiplicity was used:

$$\sigma_\nu(A,Z,A_c) = 0.75 + 0.21\overline{\nu}(A,Z,E_c). \tag{6}$$

In the scission-point fission model, the averaged fission characteristics are defined at the scission line corresponding to the minimum of the potential-energy surface in the multidimensional space of collective coordinates, describing an axially symmetric configuration of two nascent fragments. This collective coordinate space is comprised of three deformation parameters (quadrupole, octupole, and hexadecapole deformation types) for each of the fragments, the fragment mass and charge asymmetry parameters and the distance between the fragment tips. In our calculations, the standard Strutinsky shell-correction method [16] was applied using the parametrization of nuclear shapes according to Ref. [17]. The single-particle spectra were calculated in the axially deformed Woods-Saxon potential with the "universal" nuclear potential parameters proposed in Ref. [18]. This type of calculation was used to determine the parameters of the charge distribution of the isobaric chain. However, for calculations of the neutron-multiplicity distribution from individual primary fragments, this approach does not provide the necessary accuracy. For this purpose, a simplified version of the scission-point model with the adjusted shell-correction values [19] was used. The shell corrections as a function of the primary-fragment mass for the thermal-neutron-induced fission of ^{235}U and for the ^{252}Cf spontaneous fission were determined by a comparison with experimental neutron-multiplicity data. For other actinide compound nuclei, shell corrections at the scission point were calculated by linear interpolation and extrapolation using the mentioned reference values.

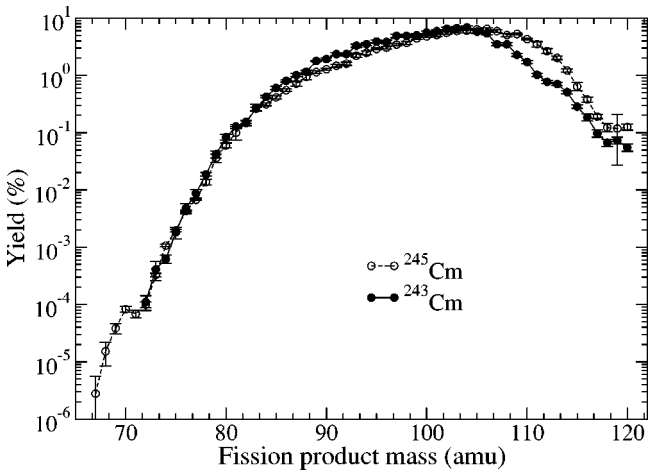

FIG. 3. Absolute mass yields for the light-mass peak from the reactions ^{243}Cm(n_{th},f) (this work) and ^{245}Cm(n_{th},f) [2,4]. The uncertainties shown are equivalent to one standard deviation.

IV. RESULTS AND DISCUSSION

A. Mass yields

Experimental results on the fragment-mass distribution are displayed in Fig. 3, along with the data for the ^{245}Cm isotope [2,4]. As seen from Fig. 3, the mass curves for the two Cm isotopes behave in a quite similar manner in relation to the mass number. The only significant difference between the two curves is for masses $A>107$, near the symmetric mass partition. Here, the difference in the yields between ^{243}Cm and ^{245}Cm is the most pronounced; it reaches a factor of 4 for masses around $A=110$. The higher yields for the ^{245}Cm target in this region are compensated by lower yields at $A=85-100$, where the yield of ^{243}Cm is slightly stronger. The effect of changes in mass yields with isotopic mass of a compound nucleus is well known from spontaneous fission—for example, as seen in the Pu isotopes [20]. One can also see the same behavior of the mass-yield curve in the data of the Cm isotopes (see, e.g., Ref. [21]).

The proximity of the mass curves in the superasymmetric mass region ($A<80$) clearly visible in Fig. 3 is not acciden-

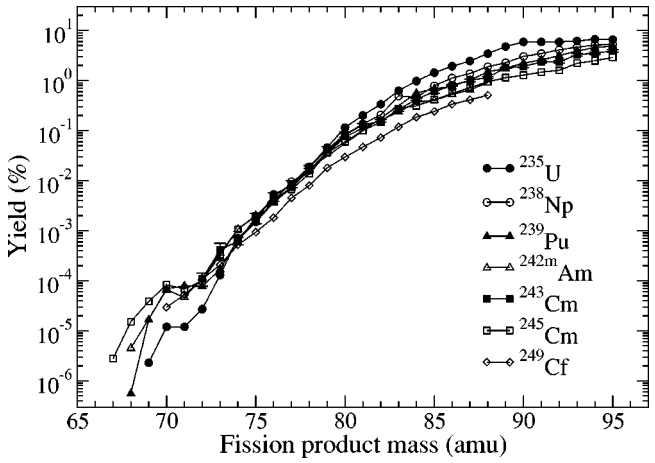

FIG. 4. Absolute mass yields for the light-mass peak from the reactions ^{235}U(n_{th},f) [22,23], ^{237}Np(n_{th},f) [8,24], ^{239}Pu(n_{th},f) [25,26], ^{242m}Am(n_{th},f) [27], ^{243}Cm(n_{th},f) (this work), ^{245}Cm(n_{th},f) [2,4], and ^{249}Cf(n_{th},f) [28]. The error bars (1σ) are shown only for ^{243}Cm.

tal; it appears to be a general feature in low-energy fission (see Fig. 4). This behavior of fission-yield curves was disclosed quite recently, when data in the superasymmetric mass region became available for various compound nuclei and were compared [8]. As seen from Fig. 4, for $A<80$, the yield of masses from various fissioning systems is practically the same. The mass coincidence takes place over a broad mass interval and—what is even more remarkable—it persists over a large range of mass yields (approximately three orders of magnitude). The intersection of the yield curves in the light-mass peak is attributable to the combined action of two shell closures ($Z=28$ and $N=50$). Unlike the doubly magic ^{132}Sn case, the two shells do not belong to the same fragment but are displaced from each other by approximately 12 masses. This displacement can be a reason for such a "prolonged" overlap in mass yield observed for all compound nuclei studied so far at Lohengrin. A small deviation from the common trend seems to be present for ^{249}Cf. However, this can be caused by a yield normalization, since only a fraction of the light-mass peak had been measured. It has to be noticed that the stabilizing role of the shells appears to be strong enough to transform the behavior of the mass-yield curves, which are known to exhibit different slopes near the top of the mass peak (Fig. 4).

The proximity of the yield means that the formation probability of very light fragments is not sensitive to the difference in excitation energy, which appears from the difference in neutron-binding energy for the compound nuclei under consideration. This implies that such fragments are formed in a cold state and have nearly spherical shapes at the scission point. A physical quantity related to the fragment's excitation and deformation is the corresponding prompt-neutron multiplicity. Unfortunately no reliable experimental data on prompt-neutron emission are available to make a definitive conclusion on this subject.

The independence of the mass yield from the fissioning system, established in the superasymmetric mass region for thermal-neutron-induced fission, as well as the anomalous behavior of the the fission-yield curve around $A=70$ (see, e.g., [2]), strongly supports the necessity to consider additional modes in the multimodal approach as mentioned earlier in Eq. (3). We applied the formalism described in Sec. III to the ^{243}Cm and ^{245}Cm nuclei, to calculate the yield of masses and of individual isotopes. The parameters of the fission modes were determined, too, by a comparison with product yields measured in ^{243}Cm(n_{th},f) and ^{245}Cm(n_{th},f) reactions.

However, the fission-mode parameters obtained from systematics developed for intermediate compound-nucleus excitations [12] could not be used directly for the case of low energies, since they are expected to fluctuate for different compound nuclei. Consequently, only the mean-mass values A_i of the modes have been calculated using phenomenological relations from Ref. [12]; the mode variations were determined by a comparison with the experimental mass-yield data. The anharmonicity-correction coefficients c_i [Eq. (4)] in the calculation were fixed with the exception of three, whose values were adjusted. In addition to these eight free parameters, the mode weight coefficients C_i [see Eq. (3)] were determined for each compound nucleus, with their sum being normalized to 100%. All the parameters are listed in Table I. The steepness with which the mass-yield curve decreases towards the symmetric region defines the anharmonicity-correction coefficient for both standard modes; the structure in the mass-yield curve at $A=70$ in ^{245}Cm imposes a strong limitation on the $c^{\rm as}_{\rm SII}$ coefficient. Though the mode at $A=70$ is narrow and its contribution to the total yield is small, the structure at $A=70$ is important for understanding the superasymmetric fission dynamics. In the ^{243}Cm($n_{\rm th},f$) case, there are no experimental data near A

TABLE I. Fission-mode parameters for ^{243}Cm and ^{245}Cm. For each isotope and for each mode, average mass A_i, standard deviation $\sigma^i(A_i)$, and coefficients c_i (c^{as} and c^{sy}) are given according to Eq. (4).

	^{243}Cm					^{245}Cm				
Mode	A_i (amu)	$\sigma^i(A_i)$ (amu)	c^{as}	c^{sy}	C_i (%)	A_i (amu)	$\sigma^i(A_i)$ (amu)	c^{as}	c^{sy}	C_i (%)
SY	122.00	8.9(1)	0.00	—	1.14(5)	123.00	8.94(10)	0.00	—	2.20(1)
SI	132.71	4.8(1)	0.00	0.40(2)	0.03(1)	132.32	3.56(10)	0.00	0.60(2)	13.4(2)
SII	141.78	9.5(1)	0.10(1)	0.25(1)	98.7(5)	141.04	9.73(10)	0.08(1)	0.30(1)	84.00(5)
SA1	82.00	1.17(5)	0.00	0.00	0.11(1)	82.00	1.17(5)	0.00	0.00	0.34(2)
SA2	70.00	0.60(5)	0.00	0.00	$6.6\times10^{-5}(5\times10^{-6})$	70.00	0.60(5)	0.00	0.00	$1.0\times10^{-4}(2\times10^{-6})$

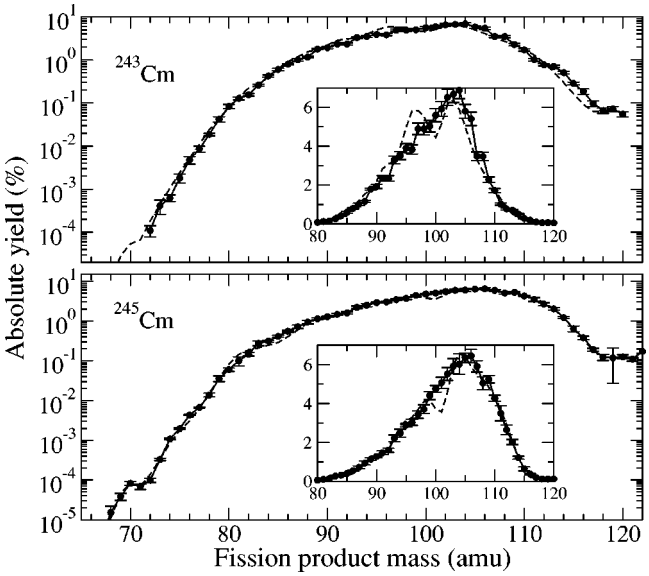

FIG. 5. Comparison between experimental (connected points) and calculated (dashed lines) mass yields for ^{243}Cm and ^{245}Cm. The insets are the same data but on a linear scale.

=70 and further experiments are needed to check our predictions in this nucleus. The effect of the weak *SA*1 mode connected with the nuclear shell $N=50$ manifests itself in the form of a change in the mass-curve slope near $A=80$ [8].

An important feature to note is that the fraction of the ^{78}Ni mode (*SA*1 and *SA*2) increases from ^{243}Cm to ^{245}Cm. The contribution of the symmetric mode (*SY*) to the mass yield seems to increase too, with increasing isotopic mass, which correlates with the mass-yield behavior in the symmetry (Fig. 3). It is desirable to measure mass yields in the whole valley region to make definitive conclusions on the importance of this mode for the valley-region population in ^{243}Cm and on the corresponding peak-to-valley ratios. The most surprising finding is, however, the disappearance of the standard-*I* (SI) mode in ^{243}Cm. Certainly, this mode is too neutron excessive to be competitive in the fission of ^{243}Cm.

In Fig. 5, a comparison is presented between experimental and calculated data for the light-mass peak for the two Cm isotopes. One sees a good description of the experimental curves by the model, apart from the $A=100$ region where the theoretical curves show an additional, but relatively small, structure. This disagreement can be explained by a specific dependence of the neutron multiplicity on the fragment mass and charge. Common procedure and parameters were used to calculate the multiplicity of prompt neutrons emitted from primary fragments (see Sec. III). In Fig. 6, the neutron-multiplicity curves are compared for the ^{244}Cm* and ^{246}Cm* compound nuclei, as a function of the primary-fragment mass. In general, these curves are almost identical; some differences between them can be explained by the difference in neutron binding energies and excitation energies of the primary fission fragments.

B. Isotopic and isobaric yields

Absolute yields of individual nuclei were obtained as a product of the absolute mass yields $[Y(A)]$ and fractional

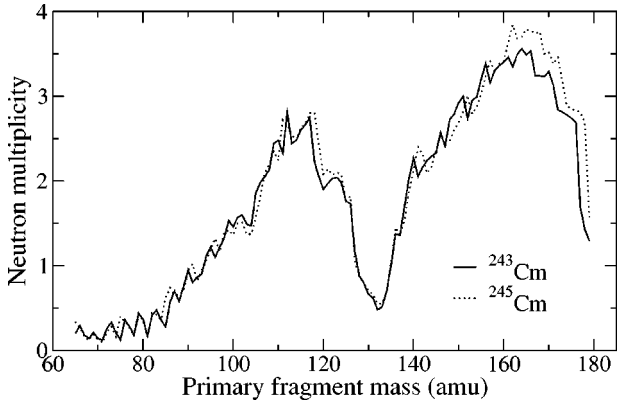

FIG. 6. Calculated prompt-neutron multiplicities used in the yield calculations for the ^{243}Cm (solid line) and ^{245}Cm (dotted line) targets.

independent yields $[\mathrm{FIY}(A,Z)]$. The latter were obtained from the evaluation of the specific energy losses ΔE of fission fragments in the ionization chamber. Since the nuclear charge resolving power of gaseous detectors does not exceed $Z/\Delta Z=40$, a reliable identification of isobars was possible only in a relative short mass range (up to $A=90$).

With extracted fission-mode parameters (see Table I), the independent fission-product yields were calculated. The calculated and experimental isotopic yields in the fragment-charge-number interval $Z=28-37$ for the ^{243}Cm target are compared in Fig. 7. One can see that the agreement between experimental and theoretical values is very good. This proves the validity of the model of a frozen quantal fluctuation for the calculations of the mean charge and charge dispersion of the isobaric chain.

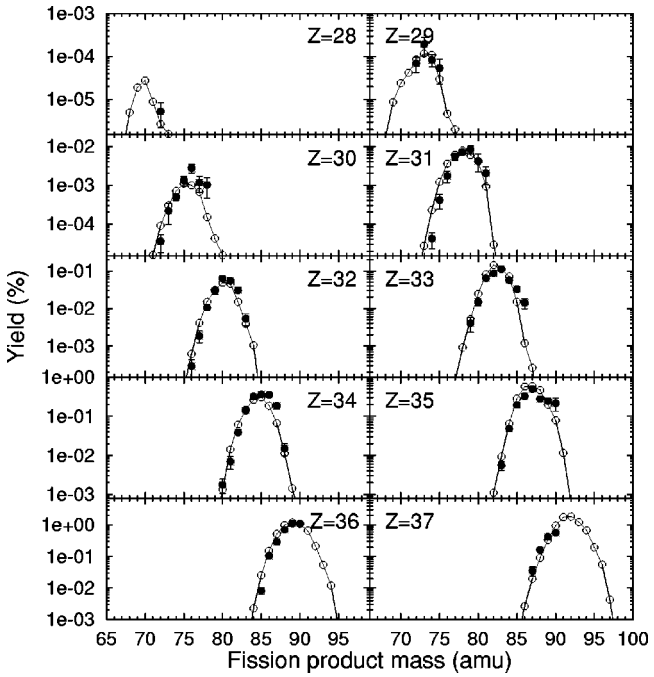

FIG. 7. Comparison between experimental (solid points) and calculated (open points) isotopic distributions from the ^{243}Cm(n_{th},f) reaction.

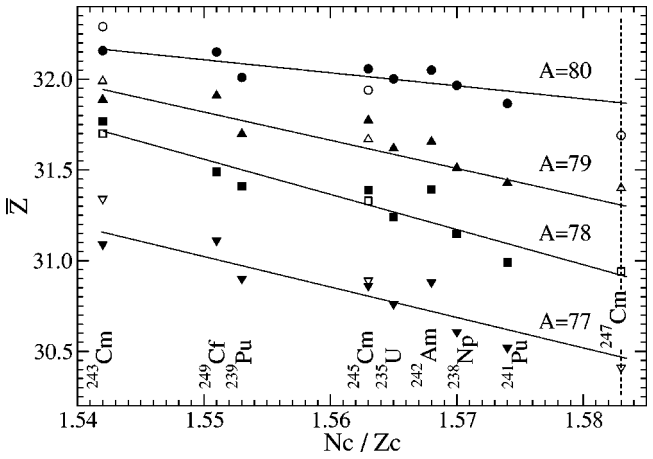

FIG. 8. Experimental (solid points) and calculated (open symbols) mean isobaric charge $\overline{Z}$ for masses $A=77-80$, obtained from the thermal-neutron-induced fission of different nuclei, as a function of the neutron-to-proton ratio of the corresponding compound systems. The data for ^{241}Pu were taken from [4]; for other references, see Fig. 4. The straight lines are for legibility only.

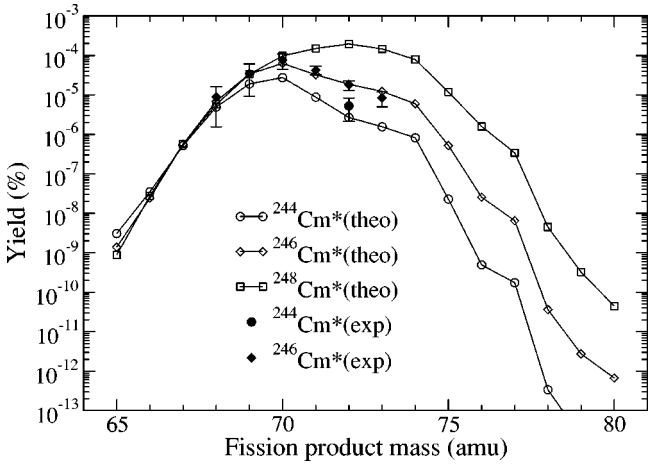

FIG. 9. Calculated absolute yields of Ni isotopes from fission of the ^{244}Cm*, ^{246}Cm*, and ^{248}Cm* compound nuclei. Black points are the experimental data.

The prediction of yields of extremely-neutron-rich fission products, such as ^{78}Ni, is a challenging task. Here, we have investigated the systematic trends in the dependence of the mean charge in the $A=77-80$ isobaric chains using the Lohengrin experimental data. In Fig. 8, the experimental mean-charge values $\overline{Z}$ for the $A=77-80$ isobaric chains as a function of the neutron-to-proton ratio of the compound nuclei for the thermal-neutron-induced fission of targets from U to Cf are presented as solid symbols. Since for these isobaric chains the experimental data are available only for limited charge numbers (3 or 4), the extraction of the charge dispersions and of the uncertainties of $\overline{Z}$ with a high confidence level is impossible. The error for the $\overline{Z}$ was estimated to be equal to about 0.3, since the uncertainties for independent-product yields in this mass region are in the order of 10% or less. One can see that the dependence $\overline{Z}(Nc/Zc)$ for a certain isobaric chain can be approximated by a straight line. The calculated $\overline{Z}$ values for the ^{244,246,248}Cm* compound nuclei (open symbols in Fig. 8) follow the experimental trend.

Based on the overall good agreement between theoretical and experimental data we could predict yields of neutron-rich Ni isotopes. Calculated independent yields of the Ni isotopes in the thermal-neutron-induced fission of the ^{243,245,247}Cm targets along with available experimental data are presented in Fig. 9. As appears from Fig. 9, there is a remarkable difference in yield between the three compound systems studied, for the heavy Ni isotopes. The gap in yields, however, vanishes for light Ni isotopes. This is a consequence of the shift of the isobaric distribution towards smaller nuclear charges, with increasing isotopic mass, and of the focusing effect of the superasymmetric fission mode on the mass-yield curve behavior in the corresponding mass region.

A point of special interest in Fig. 9 is the yield of ^{78}Ni. The ^{78}Ni nucleus is one of a few nuclei of key importance in the understanding of stellar nucleosynthesis. Though ^{78}Ni was already observed quite a long time ago [29], the excess of 22 neutrons in this nucleus strongly prohibits its production in quantities required for spectroscopic studies. Neutron-induced fission is doubtless one of the possible reactions capable of producing ^{78}Ni, since it preserves and even increases, by adding one more neutron to the target nucleus, the neutron-to-proton ratio of fission fragments. As follows from Figs. 8 and 9, thermal-neutron-induced fission of ^{247}Cm appears to be a very promising reaction for the production of nuclei with extreme neutron excess.

The level of sensitivity currently reached at the Lohengrin mass separator is of the order of $\sim 10^{-7}$% [30] and corresponds to about a half day of measuring time with a transuranium target of a few tens of micrograms. The yield of 4.5×10^{-9}% estimated for ^{78}Ni from the ^{247}Cm target would mean much longer measuring times, provided the target material is available in a quantity of ~ 1 mg. Under these conditions, the ^{78}Ni count rate is expected to be several events per week of measuring time. This shows the feasibility of the ^{78}Ni yield determination at Lohengrin.

V. CONCLUSION

In conclusion, for the first time the mass and charge distributions of fission products in the thermal-neutron-induced fission of ^{243}Cm have been investigated at the Lohengrin mass separator. Fission-product-mass yields were measured in the mass interval $A=72-120$, reaching a yield value of about 10^{-4}% for the superasymmetric mass division. Independent yields of individual nuclei were determined for the fission-product masses below $A=90$ and in the charge interval $Z=28-37$.

Stabilization of the left wing of the light-mass peak in the superasymmetric mass region discovered in other reactions at Lohengrin (see Fig. 4 for references) was also confirmed in the reaction under consideration. This feature of the mass curve, along with the discontinuity in yield disclosed at mass $A=70$ (Fig. 4), strongly supports the hypothesis on the important role of nuclear shells $Z=28$ and $Z=50$ in superasym-

metric fission [31]. Contrary to the ^{132}Sn mode with $Z=50$ and $Z=82$, the influence of the $Z=28$ and $Z=50$ shells spans a wide range of masses, since any coherent action of the doubly magic ^{78}Ni mode is prohibited by a large deviation of its neutron excess from that of the compound nuclei.

The multimodal fission approach and the model of frozen quantal fluctuations of charge asymmetry at the scission point were used for fission-product yield calculations. To describe the lightest slope of the mass peak, the two superasymmetric fission modes (at $A=82$ and $A=70$) were introduced to the calculation. The reliability of the method's predicting power has been demonstrated by the agreement between calculated and experimental data on the ^{243}Cm and ^{245}Cm isotopes. The parameters of fission modes were extracted for the ^{244}Cm* and ^{246}Cm* compound nuclei. It was found that the weight of the standard-I mode (^{132}Sn mode) for the ^{244}Cm* compound nucleus is very small in comparison with that for the ^{246}Cm* compound system. It is a common trend that the weight of the ^{132}Sn mode increases with the increasing neutron-to-proton ratio of a compound system (Nc/Zc). This feature was used to predict fission-product yields in the reaction ^{247}Cm(n_{th},f), which was shown to be very promising for production of nuclei with extreme neutron excess.

The systematics obtained for the mean-product charge of the isobaric chains $A=77-80$ for compound nuclei from ^{236}U* to ^{250}Cf* measured at Lohengrin demonstrates a clear decrease of $\overline{Z}$ as the ratio Nc/Zc increases. This systematics is very useful for predicting and testing theoretical models. Predictions of yields of neutron-rich Ni isotopes were made for the ^{244}Cm*, ^{246}Cm*, and ^{248}Cm* compound nuclei formed after capture of thermal neutrons. The cross section for the ^{78}Ni formation in the thermal-neutron-induced fission of ^{247}Cm is predicted to be about 4 nb. This is higher by one order of magnitude than the value obtained in fission induced by peripherical collisions of 750 MeV/nucleon projectiles of ^{238}U on a Be target [29]. This yield level for ^{78}Ni is promising for planning new experiments at Lohengrin.

ACKNOWLEDGMENTS

The interest in this work shown by Dr. F. Storrer from the CEA Saclay is gratefully acknowledged. The stay of one of the authors (N.V.) at the ILL was supported by NATO.

[1] E. Moll, H. Schrader, G. Siegert, H. Hammers, M. Asghar, J. P. Bocquet, P. Armbruster, H. Ewald, and H. Wollnik, Kerntechnik **19**, 374 (1977).
[2] D. Rochman, I. Tsekhanovich, F. Gönnenwein, V. Sokolov, F. Storrer, G. Simpson, and O. Serot, Nucl. Phys. **A735** 3 (2004).
[3] C. D. Bowman, E. D. Arthur, P. W. Lisowski, G. P. Lawrence, R. J. Jensen, J. L. Anderson, B. Blind, M. Cappiello, J. W. Davidson, T. R. England, L. N. Engel, R. C. Haight, H. G. Hughes, J. R. Ireland, R. A. Krakowski, R. J. LaBauve, B. C. Letellier, R. T. Perry, G. J. Russell, K. P. Staudhammer, G. Versamis, and W. B. Wilson, Nucl. Instrum. Methods Phys. Res. A **320**, 336 (1992).
[4] T. Friedrichs, Ph.D. thesis, Technical University of Braunschweig, Germany, 1998.
[5] U. Brosa, S. Grossmann, and A. Müller, Phys. Rep. **197**, 167 (1990).
[6] J. P. Biersack and J. F. Ziegler, computer code TRIM. Freeware, available at http://www.srim.org
[7] G. Pfennig, H. Klewe-Nebenius, and W. Seelmann-Eggebert, *Chart of the Nuclei*, 1995, http://ie.lbl.gov/ngdata/sig.htm
[8] I. Tsekhanovich, H. O. Denschlag, M. Davi, Z. Büyükmumcu, F. Gönnenwein, S. Oberstedt, and H. R. Faust, Nucl. Phys. **A688**, 633 (2001).
[9] V. A. Rubchenya and J. Äystö, Nucl. Phys. **A701**, 127c (2002).
[10] B. L. Tracy, J. Chaumont, R. Klapisch, J. M. Nitschke, A. M. Poskanzer, E. Roeckl, and C. Thibault, Phys. Rev. C **5**, 222 (1972).
[11] J. P. Bocquet and R. Brissot, Nucl. Phys. **A502**, 213c (1989).
[12] V. A. Rubchenya and J. Äystö, EURISOL Research Project. http://ganil.fr/eurisol/
[13] H. Nifenecker, J. Phys. (France) Lett. **41**, L47 (1980).
[14] E. S. Hernandez, W. D. Myers, J. Randrup, and B. Remaud, Nucl. Phys. **A361**, 483 (1981).
[15] I. D. Alkhazov, B. F. Gerasimenko, A. V. Kuznetsov, B. F. Petrov, V. A. Rubchenya, and V. I. Shpakov, Yad. Fiz. **48**, 1635 (1988).
[16] V. M. Strutinsky, Nucl. Phys. **A122**, 1 (1968).
[17] V. V. Pashkevich, Nucl. Phys. **A169**, 275 (1971).
[18] S. Cwiok, J. Dudek, W. Nazarewicz, J. Skalski, and T. Werner, Comput. Phys. Commun. **46**, 379 (1987).
[19] P. P. Jauho, A. Jokinen, M. Leino, J. M. Parmonen, H. Penttila, J. Äystö, K. Eskola, and V. A. Rubchenya, Phys. Rev. C **49**, 2036 (1994).
[20] L. Demattè, C. Wagemans, R. Barthélémy, P. D'hondt, and A. Deruytter, Nucl. Phys. **A617**, 331 (1997).
[21] F. Caïtucoli, M. Asghar, B. Leroux, G. Barreau, K. Hamadache, A. Sicre, T. P. Doan, and M. Allab, Nucl. Phys. **A394**, 360 (1993).
[22] J. L. Sida, P. Armbruster, M. Bernas, J. P. Bocquet, R. Brissot, and H. R. Faust, Nucl. Phys. **A502**, 233 (1989).
[23] W. Lang, H. G. Clerc, H. Wohlfahrth, H. Schrader, and K. H. Schmidt, Nucl. Phys. **A345**, 34 (1980).
[24] G. Martinez, G. Barreau, A. Sicre, T. P. Doan, B. Leroux, W. Arafa, R. Brissot, J. P. Bocquet, H. R. Faust, P. Koczon, M. Mutterer, F. Gönnenwein, M. Asghar, U. Quade, K. Rudolph, D. Engelhardt, and E. Piasecki, Nucl. Phys. **A515**, 433 (1990).
[25] W. Ditz, Ph.D. thesis, University of Mainz, Germany, 1991.
[26] C. Schmitt, A. Guessous, J. P. Bocquet, H. G. Clerc, R. Brissot, D. Engelhardt, H. R. Faust, F. Gönnenwein, M. Mutterer, H. Nifenecker, J. Pannicke, Ch. Ristori, and J. P. Theobald, Nucl. Phys. **A430**, 21 (1984).
[27] I. Tsekhanovich, H. O. Denschlag, M. Davi, Z. Büyükmumcu, M. Wöstheinrich, F. Gönnenwein, S. Oberstedt, and H. R. Faust, Nucl. Phys. **A658**, 217 (1999).
[28] R. Hentzschel, H. R. Faust, H. O. Denschlag, B. D. Wilkins,

and J. Gindler, Nucl. Phys. **A571**, 427 (1994).
[29] Ch. Engelmann, F. Ameil, P. Armbruster, M. Bernas, S. Czajkowski, Ph. Dessagne, C. Donzaud, H. Geissel, A. Heinz, Z. Janas, C. Kozhuharov, Ch. Miele, G. Münzenberg, M. Pfutzner, C. Rohl, W. Schwab, C. Stephan, K. Summerer, L. Tassan-Got, and B. Voss, Z. Phys. A **352**, 351 (1995).
[30] I. Tsekhanovich, Z. Büyükmumcu, M. Davi, H. O. Denschlag, F. Gönnenwein, and S. F. Boulyga, Phys. Rev. C **67**, 034610 (2003).
[31] V. A. Rubchenya, in *Proceedings of the International Workshop on Fission Dynamics of Atomic Clusters and Nuclei, Luso, Portugal, 2000*, edited by J. da Providencia *et al.* (World Scientific, Singapore, 2001), p. 221.